INSTITUTE OF PHYSICS PUBLISHING JOURNAL OF PHYSICS: CONDENSED MATTER

J. Phys.: Condens. Matter **15** (2003) L597–L605 PII: S0953-8984(03)65258-6

LETTER TO THE EDITOR

Impact of self-irradiation damage on the aqueous durability of zircon ($ZrSiO_4$): implications for its suitability as a nuclear waste form

Thorsten Geisler[1,2], Kostya Trachenko[2], Susana Ríos[2], Martin T Dove[2] and Ekhard K H Salje[2]

[1] Institut für Mineralogie, University of Münster, Corrensstraße 24, D-48149 Münster, Germany
[2] Department of Earth Sciences, University of Cambridge, Downing Street, Cambridge CB2 3EQ, UK

Received 24 June 2003
Published 8 September 2003
Online at stacks.iop.org/JPhysCM/15/L597

Abstract

Zircon has been proposed as a nuclear waste form to safely encapsulate weapons-grade plutonium. In order to study the impact of self-irradiation damage in zircon on its aqueous durability, we performed a hydrothermal experiment (2 M $CaCl_2$ solution, 600 °C, 100 MPa) with several variably radiation-damaged, i.e. amorphized, zircon samples. We found an anomalous increase in the alteration rate at two critical concentrations of amorphous domains. The first dramatic increase sets in when the amorphous domains form interconnected clusters in the structure. The second increase is related to the percolation of fast diffusion pathways consisting of nano-sized regions of depleted matter that are formed during strongly overlapping α-recoil events, as seen by molecular-dynamics simulations and small-angle x-ray scattering measurements. The two percolation thresholds provide model benchmarks for the safety performance of a zircon waste form.

M This article features online multimedia enhancements

The safe disposal of highly radioactive materials, including high-level nuclear waste and plutonium from civil reactors and the dismantling of nuclear weapons, is a pressing issue in modern society due to the enormous amounts of radioactive waste that have been accumulated world-wide during the past decades [1]. Zircon ($ZrSiO_4$) and more complex ceramics such as, e.g., pyrochlore, perovskite, and zirconolite, which are part of the Synroc ceramic waste form, have been proposed to safely encapsulate highly radioactive waste [1, 2]. Zircon is also widely used in geochronology and has recently become a model 'host' matrix for studying encapsulation of plutonium waste in ceramic materials [1, 3].

The propagation of the heavy recoil generated during the radioactive decay of U, Th, or Pu, substituting Zr^{4+} in zircon, causes a transformation from the crystalline to a topologically

disordered, amorphous ('metamict') state [4, 5]. The radiation damage process is characterized by a continuous transition from a structural state that is characterized by amorphous islands randomly located in the crystalline environment to a microstructure where isolated crystalline domains are located in an amorphous matrix [4–10]. These microstructural changes are accompanied by large volume and unit-cell swelling [4–6], shear deformation [11], and the formation of a polymerized phase [12–14]. It is well known that such irradiation damage effects change the bulk physical properties of zircon, including a decreased stability against aqueous solutions as the degree of damage increases [15]. We have previously demonstrated that treatment of radiation-damaged zircon in hydrothermal aqueous solutions produces a rim of recrystallized zircon, which forms behind a sharp reaction front [16–18]. The moving recrystallization front is the result of inward diffusion of water (H^+ and molecular water), which drastically reduces the activation energy to solid state recrystallization. Evidence for a diffusion-based recrystallization process is, for example, the observation of intermediate, temperature-dependent structural recovery states, precluding a dissolution–reprecipitation mechanism as a rim forming process. However, a thorough understanding of the impact of self-irradiation damage on the stability of zircon and other potential nuclear waste form materials against hydrothermal aqueous solutions is still lacking, but is indispensable to predict their stability with increasing storage time under a given waste loading.

In order to study the aqueous durability of zircon as a function of its degree of self-irradiation damage, we carried out a hydrothermal experiment with 16 gem-type, variably coloured, alluvial zircon crystals from Sri Lanka. The sample set covers a broad range of radiation damage, as reflected by their U and Th concentrations and Raman spectroscopic measurements (table 1). With increasing p the zircon samples are characterized by a decrease of the frequency of the asymmetrical $\nu_3(SiO_4)$ band and an increase of its width, which is in agreement with previous Raman studies on radiation-damaged zircon [19]. The amorphous fraction p, estimated from the α-decay dose (see table 1), ranges from 0.02 to 0.95. The hydrothermal experiment was carried out with a single fragment from each of the samples in a 2 M $CaCl_2$ solution at 600 °C and 100 MPa water pressure for 72 h. A temperature of 600 °C is much higher than one would expect even in deeply buried nuclear waste repositories, but was chosen to accelerate the reaction process especially in the less metamict samples. We note, however, that dry annealing experiments with metamict zircon have shown that epitaxial recrystallization is not activated at 600 °C [20, 21], i.e. that p does not change during the experiment in those areas that have not reacted with the fluid. The fragments used for the experiment have been carefully polished to form a single flat surface. In order to assure identical experimental conditions, all fragments were placed in a single 4 cm long gold capsule after being photographed along with 2 ml of a 2 M $CaCl_2$ solution. The gold capsule was placed at the hot spot of a standard cold-seal hydrothermal pressure vessel. The pressure and temperature were constant within ±5 MPa and ±2 °C, respectively. After the experiment, the grains were carefully washed in distilled water in an ultrasonic bath to remove any $CaCl_2$ from the reacted surface before the grains were embedded in epoxy resin and polished to about half their thickness perpendicular to the polished face. The experimental products were characterized by optical microscopy, backscattered electron (BSE) and Ca Kα x-ray imaging as well as by micro-Raman spectroscopic measurements.

After the experiments, all samples with $p < 0.75$ are transparent (figures 1(a)–(f)), whereas the four most metamict grains ($p > 0.75$) are milky-white (figures 1(g) and (h)). Below $p \approx 0.3$ the zircon fragments appear virtually unaltered. Slightly rounded edges, however, may indicate that minor congruent dissolution took place (figure 1(i)). However, those zircon grains with $p > 0.3$ have intensively reacted with the fluid, as indicated by sharply bounded, Ca-rich reaction rims up to a thickness of 35 μm (figures 1(j)–(n) and (q)–(u)).

Table 1. Electron microprobe and Raman spectroscopic data of the untreated samples and the experimental products. The measured minimum, x_{min}, and maximum, x_{max}, reaction rim thickness is also given. n.m. reaction rim too small to be measured.

	Starting material						Reacted areas				
Sample	U (ppm)	Th (ppm)	D[a]	p[b]	ω[c] (cm^{-1})	Γ[c] (cm^{-1})	Ca (ppm)	x_{min} (μm)	x_{max} (μm)	ω_r^c (cm^{-1})	Γ_r^c (cm^{-1})
Z11[d]	252	114	0.56	0.02	1008.3	2.2					
Z13	257	227	0.61	0.04	1006.1	4.8					
Z1	495	<70	0.99	0.13	1004.0	7.3	A reaction rim could				
CZ24[d]	626	132	1.27	0.20	1003.1	9.6	not be detected ($x \lesssim 0.3$ μm)				
Z2	694	220	1.48	0.25	1001.9	10.3					
Z3	791	210	1.67	0.28	1000.4	12.8					
HZ4	1081	199	2.15	0.37	999.2	15.9	n.m.	0.4	0.6	n.m.	n.m.
HZ6[e]	1573	303	3.09	0.52	1002.3	13.0	n.m.	1.0	1.6	n.m.	n.m.
Z12	1544	273	3.20	0.53	997.6	19.2	n.m.	1.5	2.5	n.m.	n.m.
Z16[d]	1997	627	4.26	0.65	995.8	25.4	1530	1.0	12.0	1002.8	23.8
HZ5	2396	701	4.82	0.70	996.0	30.2	4950	10.0	16.5	1005.4	11.9
Z9	2583	515	4.98	0.72	997.1	31.9	6700	31.0	35.0	1006.7	7.3
CZ25	2750	860	5.86	0.78	997.5	31.9	4980	$\gtrsim$120		1007.1	6.4
No2	3400	98	6.77	0.83	Crystalline signals		7100	$\gtrsim$170		1007.3	5.3
3	4074	455	7.80	0.87	not detectable		8700	$\gtrsim$160		1007.1	7.1
HZ7	5647	317	11.39	0.95	anymore		8130	$\gtrsim$150		1007.1	9.8

[a] D represents the α-decay dose ($\times 10^{18}$, in α-decays g^{-1}), which was calculated from the U and Th concentration measured by electron microprobe and an age of 570 Ma [36].

[b] p is the amorphous fraction, which was estimated from the α-decay dose D and $p = 1 - \exp(-B(D - D_{inc}))$ with $B = 0.28(1) \times 10^{-18}$ g and an incubation dose $D_{inc} = 0.47(8) \times 10^{18}$ α-decays g^{-1}. The parameters B and D_{inc} were obtained by a new fit to published experimental data [8, 12, 13]. D_{inc} accounts for annealing during the geological history of the samples.

[c] ω and Γ represent the frequency and the corrected linewidth (full width at half maximum) of the asymmetrical $\nu_3(SiO_4)$ stretching band near 1008 cm^{-1}, respectively. The measured linewidth has been corrected for instrumental broadening according to Tanabe and Hiraishi [37].

[d] Average U and Th concentration obtained from electron microprobe measurements on several fragments of each sample using the method of Geisler and Schleicher [38]. In all other cases the given U and Th concentration represents the average of five to ten measurements performed prior to the experiment on the same fragment as used for the experiment.

[e] The sample was probably annealed in an open fire by gem collectors to improve the colour, resulting, however, only in the partial recovery of disordered crystalline remnants [21].

At high degrees of amorphization ($p > 0.5$) the extent of the reaction could also be traced by BSE imaging due to a significantly lowered BSE intensity (figures 1(i)–(n)), indicating the occurrence of significant amounts of water (as OH and/or H_2O) in the reacted areas. The formation of cracks caused partial surface disintegration and is partly accompanied by a scalloped reaction front morphology (figures 1(i) and (m)). The four most metamict grains ($p > 0.75$) have completely reacted, which is evidenced by the occurrence of high Ca concentration within the interior of the grains (figures 1(o) and (p)) and by their milky-white appearance. The most metamict sample with $p = 0.95$ also started to disintegrate (figure 1(p)). Micro-Raman measurements on the reaction zones show that the structure was partially healed (table 1), as indicated by a blue-shift of the asymmetrical $\nu_3(SiO_4)$ stretching band and a decrease of its width [20, 21]. However, the frequency and the line shape does not resemble that of crystalline zircon, confirming previous interpretation that the reaction rims were not formed by a coupled dissolution–reprecipitation process, but must be controlled by diffusion–reaction processes [16–18].

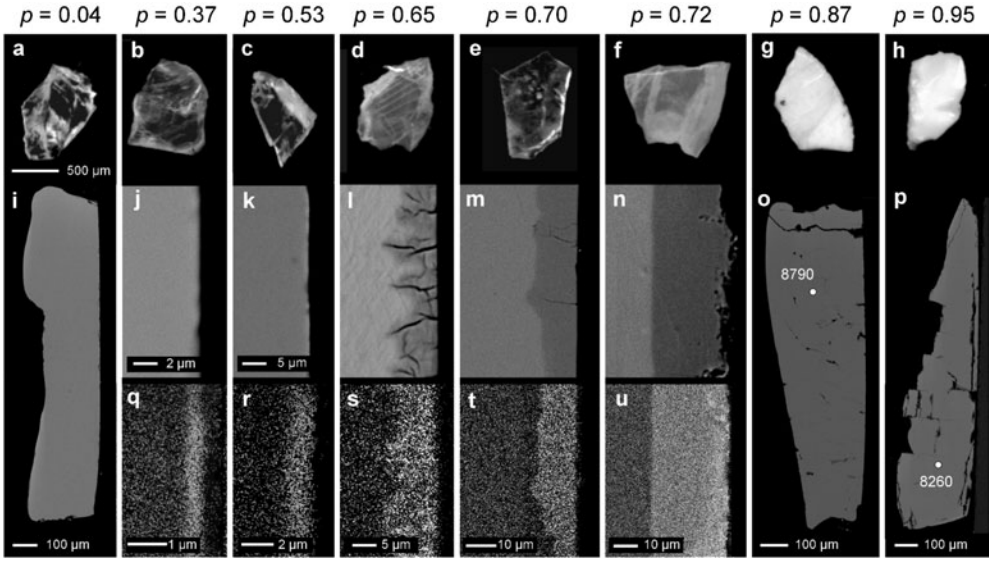

Figure 1. Optical microscope (a)–(h), BSE (i)–(p), and Ca Kα x-ray scanning images (q)–(u) of hydrothermally treated, variably radiation-damaged zircon fragments. Reacted areas are characterized by high Ca concentration and, in (i)–(m), by a lowered BSE intensity compared to the unreacted core. The polished surface, representing the zircon–fluid interface, is on the right-hand side in each BSE and Ca distribution image. Electron microprobe spot locations are shown in (o) and (p) along with the Ca concentration in ppm. (Experimental conditions: 72 h in 2 M $CaCl_2$ solution at 600 °C and 100 MPa fluid pressure.)

Figure 2 is a plot of the reaction rim thickness as a function of p. We can clearly identify a first dramatic increase of the alteration rate near $p_c = 0.3$, followed by a second dramatic increase near $p^* = 0.7$. Before addressing the origin of this behaviour, we note that compared with the very low diffusivity of water in crystalline zircon (of the order of 10^{-24} m^2 s^{-1} at 600 °C [22]) the large apparent diffusion distance of water observed in the most metamict grains, as approximated by the rim thickness, x, is remarkable. This becomes even more evident when comparing the kinetics of water diffusion in metamict zircon with those in silica glass. The most metamict grains have completely reacted, allowing only an estimate of a minimum rim thickness to be made, which is given by the smallest radius measured on half-sectioned grains (table 1). Using these values for x, we can estimate a minimum effective diffusion coefficient for water, $D^{\mathrm{eff}}_{\mathrm{water}}$, of the order of 10^{-13} m^2 s^{-1} at 600 °C, assuming that $x^2 \approx D^{\mathrm{eff}}_{\mathrm{water}} t$, where t is the duration of the experiment. $D^{\mathrm{eff}}_{\mathrm{water}}$ for silica glass was found to be of the order of 10^{-14}–10^{-15} m^2 s^{-1} [23–25], i.e. $D^{\mathrm{eff}}_{\mathrm{water}}$ for metamict zircon is even larger. This is very surprising since the ionic porosity, Z (given by $Z = 1 - V/V_c$, where V is the molar volume of atoms, and V_c is the molar bulk volume [26]), which has been shown to be the main factor controlling diffusion of molecular water in silicate minerals [26], is significantly lower for metamict zircon ($\sim$41% for a density of 3.9 g cm^{-3}) than for silica glass ($\sim$51%). We note, however, that in contrast to silica glass, which dissolves after the formation of a hydration layer under hydrothermal conditions similar to those of our experiment [23], zircon does not show evidence for significant dissolution (figure 1).

Central to understanding this unusual diffusion behaviour of zircon compared to that of homogeneous quenched silica glass is the heterogeneity of the local damaged structure, which was observed in the molecular dynamics (MD) simulations of high-energy recoils in zircon

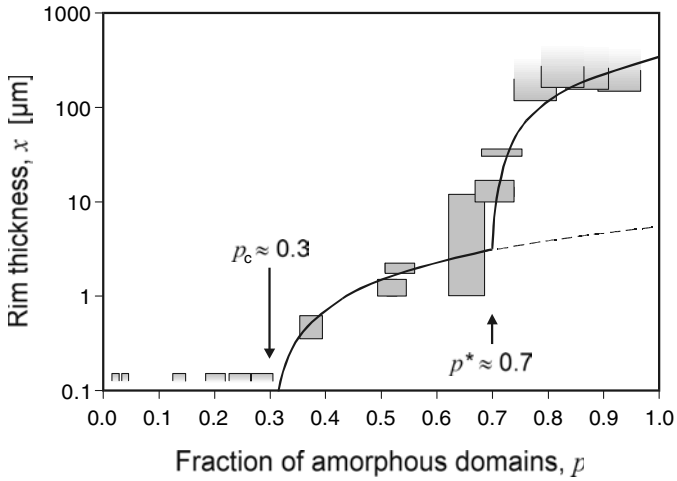

Figure 2. The reaction rim thickness, x, as a function p. The closed boxes bracket the measured minimum and maximum rim thickness and an error of 5% on the amorphous fraction. The bottom opened and top opened boxes mark the detection limit and the minimum reaction rim thickness (estimated for the completely reacted grains), respectively. Curves for $p_c > p > p^*$ and $p > p^*$ are given by $x^2 \sim (p - p_c)^z$ and $x^2 \sim (p - p_c)^z + (p - p^*)^z$, respectively, assuming $z = 2$, $p_c = 0.3$, and $p^* = 0.7$.

structure [9], and which led to the development of the percolation theory of large non-elastic volume swelling [27]. These simulations have shown that the damaged region created by an α-recoil cascade consists of a matter-depleted core surrounded by a densified boundary (figure 3(a)). The inhomogeneous density distribution in the damaged region is stabilized by the formation of a polymerized phase at the cascade boundary that consists of connected SiO_n polyhedra. Note that polymerization was also observed experimentally by ^{29}Si-NMR and IR measurements [12, 13] and was found to accompany volume swelling [4–6], which indirectly suggests the occurrence of density fluctuations.

In order to look for direct experimental evidence for the existence of density fluctuations in amorphous zircon, we have performed small angle x-ray scattering (SAXS) experiments, using a one-dimensional position-sensitive detector attached to a Mo microsource x-ray generator. Five platelet-like, variably radiation-damaged zircons ($p < 0.2$, $p = 0.55$, 0.85, 0.90, 1.0) from different sources [28–30] with thickness ranging from 0.26 to 0.56 mm have been measured. The radiation was filtered using a zirconium filter, and the x-ray beam at the sample position was 250×500 μm. The SAXS intensity was recorded as a function of the scattering vector $Q = 4\pi \sin\theta/\lambda$, where θ is the scattering angle, which ranges from $2\theta = 0.9°$ to 40°. The small angle and the wide angle regions were measured simultaneously. To obtain the SAXS intensity the background was first subtracted and then corrections for absorption were made. The degree of amorphization of these zircon samples was determined according to the method given by Ríos *et al* [8]. Figure 4 shows that as p of the sample increases, a weak signal in the small angle region ($Q < 1$ Å^{-1}) starts to develop. This signal becomes clearly distinctive in the fully amorphous specimen ($p = 1$), giving strong evidence for the presence of local density fluctuations. Within the region $QR_g < 1$, the system should follow the Guinier approximation [31], given as

$$I(Q) = I(0)\exp(-\tfrac{1}{3}R_g^2Q^2).$$

Here, R_g is the radius of gyration, which characterizes the size of the electron density fluctuations. In a Guinier plot ($\ln(I(Q)$ versus Q^2), the slope of a linear fit yields R_g

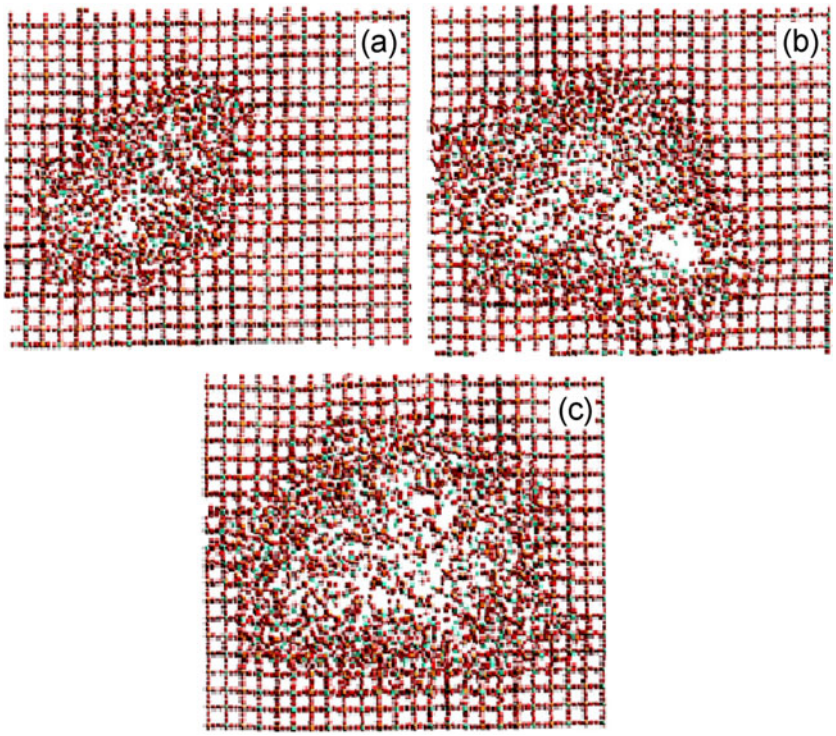

Figure 3. MD simulations of (a) a single damage cascade in zircon, showing a depleted core surrounded by a densified boundary, (b) of two, and (c) of three strongly overlapping cascades. Note the formation of interconnected regions of depleted matter in (b) and (c). (Zr atoms, blue; Si atoms, orange; O atoms, red.)

(This figure is in colour only in the electronic version)

(figure 4(b)). For the specimen with $p = 0.85$, for example, R_g was estimated to be 0.2 nm. To determine the shape of the density fluctuations, the fully amorphous sample was tilted by 90° with respect to the beam and compared to the non-tilted data. The SAXS curves were identical, suggesting that the density fluctuations are either spherical or randomly oriented. Assuming a spherical shape, the size of the density fluctuations is estimated to have a characteristic diameter of about 1 nm, which is of the order of the size of the depleted regions found in the MD simulations (∼2 nm). The SAXS results provide the first experimental confirmation of the occurrence of density heterogeneities on the nano-scale in self-irradiated amorphous zircon, as predicted in MD simulations.

We are now able to investigate the implications of the structural heterogeneities on the alteration process. We have seen that the heterogeneity of the damaged regions leads to damage scattering at the local level with percolation of the damaged phase. It was found that the percolation of the amorphous phase triggers off large volume swelling at the percolation threshold at $p_c \approx 0.3$ [27], which corresponds well to the theoretical value of the critical threshold (=0.27) in the continuum percolation problem [32]. Hence, we suggest that the first dramatic increase in diffusion and the alteration rate near $p_c = 0.3$, as seen by the penetration of Ca (figure 1), is related to large decrease in density when the damaged phase percolates. We find that in the region $0.3 < p < 0.7$ the rim thickness as a function of p can be approximated by a power law of the form $x^2 \sim (p - p_c)^z$ (figure 2), where z is given by $z = \mu - \beta \approx 2$, and

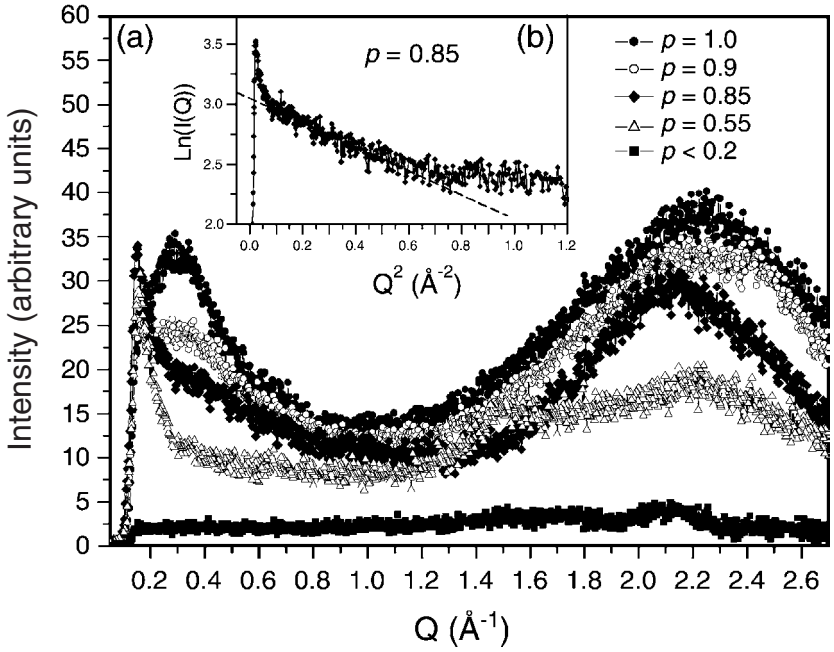

Figure 4. (a) Intensity versus scattering vector Q for five radiation-damaged zircon samples. Note the significant increase in intensity at $Q < 1$ Å^{-1} with increasing amorphous fraction, p, indicating the presence of density fluctuations. (b) The Guinier plot $\ln(I(Q))$ versus Q^2 for the sample with $p = 0.85$. The slope of the dashed line yields the radius of gyration, which characterizes the size of the density fluctuations.

μ and β are the transport exponent and the static order parameter for continuum percolation in three dimensions, respectively [33]. We note, however, that x follows power law behaviour only up to $p^* \approx 0.7$ and that in this regime the densified boundary must locally act as diffusion barriers, as shown schematically in figure 5(a).

In order to understand the second dramatic increase of the alteration rate at $p^* \approx 0.7$, we have performed further MD simulations to investigate the overlap of the damaged regions (figures 3(b), (c)). Details of the MD method, including force field and configurations, can be found in our earlier works [9, 27]. For insignificant overlap the depleted regions in two damaged regions are separated by dense shells because the recoil nucleus is reflected at the boundary of the pre-existing cascade. However, when the overlap is strong, the front of the damage cascade disperses the densified boundary of the pre-existing damage. As a result, the depleted regions connect and the damaged regions are again depleted in matter in the centre with a dense shell at their boundary (figures 3(b), (c)). This process is best seen in the animation of MD simulations in the form of mpeg movies (available in the on-line version of the journal and from http://www.esc.cam.ac.uk/movies)[3]. Based on the new MD simulations, we propose that long-range rdms are created by strongly overlapping events, which provide fast diffusion pathways.

[3] (http://www.esc.cam.ac.uk/movies/rad_per1.mpeg): This movie shows two overlapping α-decay events, but the degree of the overlap is small and the depleted regions do not connect.
(http://www.esc.cam.ac.uk/movies/rad_per2.mpeg): This movie shows two α-decay events, but now the depleted areas open up.
(http://www.esc.cam.ac.uk/movies/rad_per3.mpeg): This movie shows a third α-decay event closely overlapping with the damage produced by the two events shown in movie 2. Again the depleted areas open up.

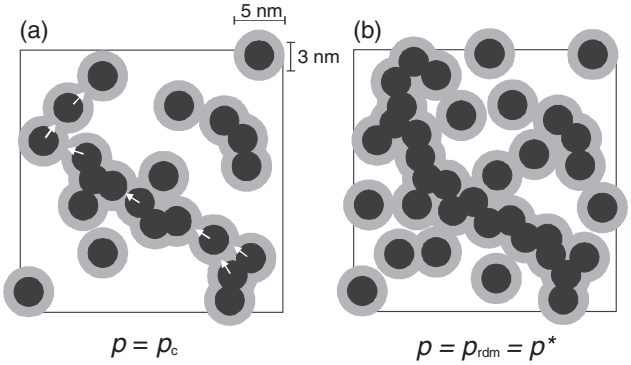

Figure 5. Schematic pictures illustrating the effect of overlapping damage cascades in zircon on its stability against hydrothermal solutions. (a) Percolation of the damaged regions, accompanied by a large density increase at $p = p_c$, causes the first dramatic increase of the alteration rate. In this regime densified boundary regions probably serve as diffusion barriers, which have to be overcome by depolymerization reactions (indicated by white arrows). (b) At $p = p^*$ interconnected regions of depleted matter (rdms, shown in figures 3(b) and (c)) provide fast diffusion pathways, resulting in a second dramatic increase of the alteration rate.

In this picture, p^* marks a point at which rdms form percolating clusters, allowing invasion-like penetration of water and other species such as Ca^{2+} over macroscopic length scales (figure 5(b)). We find that for $p > p^*$, $x^2 \sim (p - p_c)^z + (p - p^*)^z$ (figure 2), which supports the idea of a percolation-type behaviour of the alteration process.

Before concluding, it should be noted that the transport of water and other chemical species in metamict zircon was found to be coupled to solid state recrystallization and ion exchange reactions, resulting in the removal of Si and Zr from the reacted sites [16–18]. Recrystallization of amorphous zircon causes a volume reduction (up to ∼18% [5, 6]), resulting in the formation of nano-pores behind the diffusion–reaction front [18, 34]. The formation of nano-pores increases the diffusivity of chemical species behind the front as the reaction proceeds and has probably created the milky-white colour of the reacted grains (figures 1(g) and (h)). As shown in figure 5(a) the densified, polymerized boundaries of the damaged regions still serve as local barriers to diffusion at the front between p_c and p^* (as the crystalline regions do below p_c). These boundaries have to be overcome by depolymerization reactions such as hydrolysis and ion exchange during the alteration process (see figure 5(a)). In this regime the reaction rate is thus possibly not fully controlled by diffusion, but also by depolymerization reactions.

We have shown that dramatic changes of the diffusion-based alteration rate occur at two critical amorphous fractions. The two stability thresholds in zircon provide a measure of the change of the performance of a ^{239}Pu-doped zircon waste form as a function of storage time. The amorphous fraction produced in a given time t in ^{239}Pu-doped zircon can be estimated from the p versus D calibration given by Ríos *et al* [8]. Subsequently, the cumulated α-decay dose can be calculated from $D = (A/\lambda)[1 - \exp(-\lambda t)]$, where λ is the decay constant of ^{239}Pu (9.13×10^{13} s^{-1}) and A is the activity (in Bq g^{-1}). For example, a zircon doped with 5 wt% ^{239}Pu waste and stored at 200 °C under dry conditions, where structural healing is insignificant [21], already reaches the first and second critical stability thresholds after ∼350 and ∼1500 years, respectively. We note that these are short times at a low doping level compared to the recommended long time (10^4–10^6 years) required for safe disposal of highly radioactive waste. However, we should emphasize that even amorphous zircon is by far more stable against hydrothermal solutions in terms of dissolution than silica glass, which has a high dissolution rate under hydrothermal conditions similar to those of our experiments [23].

On the other hand, particularly at low fluid temperatures (<200 °C) where structural recovery is limited, high amounts of U and Th were found to be selectively removed from the reacted sites of a partially damaged zircon sample in acidic solutions [16, 18], which has to be seriously considered when evaluating the suitability of zircon as a nuclear waste form. Our results also have fundamental implications for the safe storage of high-level nuclear waste in those Synroc compounds that show radiation-induced amorphization, namely pyrochlore, perovskite, and zirconolite [35]. Here, the percolation threshold of amorphous domains provides an universal benchmark of how long the performance of these ceramics as a safe barrier to the environment will be similar to that of the fully crystalline waste form.

The authors are indebted to R T Pidgeon, J Schlüter, and the Mineralogical Museum of the University of Hamburg, Germany, for providing the samples used in this study.

References

[1] Ewing R C 1999 *Proc. Natl Acad. Sci. USA* **96** 3432
[2] Lutze W and Ewing R C 1988 *Radioactive Waste Forms for the Future* (Amsterdam: North-Holland)
[3] Weber W J 1991 *Radiat Eff. Defects Solids* **115** 341
[4] Weber W J, Ewing R C and Wang L M 1994 *J. Mater. Res.* **9** 688
[5] Murakami T, Chakoumakos B C, Ewing R C, Lumpkin G R and Weber W J 1991 *Am. Mineral.* **76** 1510
[6] Holland H D and Gottfried D 1955 *Acta Crystallogr.* **8** 291
[7] Salje E K H, Chrosch J and Ewing R C 1999 *Am. Mineral.* **84** 1107
[8] Ríos S, Salje E K H, Zhang M and Ewing R C 2000 *J. Phys.: Condens. Matter* **12** 2401
[9] Trachenko K, Dove M T and Salje E K H 2000 *J. Appl. Phys.* **87** 7702
[10] Trachenko K, Dove M T and Salje E K H 2002 *Phys. Rev.* B **65** 180102 (R)
[11] Ríos S and Salje E K H 1999 *J. Phys.: Condens. Matter* **11** 8947
[12] Farnan I and Salje E K H 2001 *J. Appl. Phys.* **89** 2084
[13] Zhang M and Salje E K H 2001 *J. Phys.: Condens. Matter* **13** 3057
[14] Trachenko K, Dove M T and Salje E K H 2001 *J. Phys.: Condens. Matter* **13** 1947
[15] Ewing R C, Haaker R F and Lutze W 1982 *Scientific Basis for Nuclear Waste Management* vol 5, ed W Lutze p 389
[16] Geisler T, Pidgeon R T, van Bronswijk W and Kurtz R 2002 *Chem. Geol.* **191** 141
[17] Geisler T, Pidgeon R T, Kurtz R, van Bronswijk W and Schleicher H 2003 *Am. Mineral.* **88** 1496
[18] Geisler T, Zhang M and Salje E K H 2003 *J. Nucl. Mater.* **320** 280
[19] Zhang M, Salje E K H, Franan I, Graeme-Barber A, Daniel P, Ewing R C, Clark A M, Ríos S and Leroux H 2000 *J. Phys.: Condens. Matter* **12** 1915
[20] Zhang M, Salje E K H, Capitani G C, Leroux H, Clark A M, Schlüter J and Ewing R C 2000 *J. Phys.: Condens. Matter* **12** 3131
[21] Geisler T 2002 *Phys. Chem. Min.* **29** 420
[22] Watson E B and Cherniak D J 1998 *Earth Planet. Sci. Lett.* **148** 527
[23] Yanagisava N, Fujimoto K, Nakashima S, Kurata Y and Sanada N 1997 *Geochim. Cosmochim. Acta* **61** 1165
[24] Wakabayashi H and Tomozawa M J 1989 *Am. Ceram. Soc.* **72** 1850
[25] Davis K M and Tomozawa M J 1995 *Non-Cryst. Solids* **185** 203
[26] Fortier S M and Giletti B J 1989 *Science* **245** 1481
[27] Trachenko K, Dove M K and Salje E K H 2003 *J. Phys.: Condens. Matter* **15** L1
[28] Ríos S and Boffa-Ballaran T 2003 *J. Appl. Crystallogr.* **36** 1006
[29] Woodhead J A, Rossman G R and Silver L T 1991 *Am. Mineral.* **76** 74
[30] Rios S 2003 unpublished data
[31] Guinier A and Fournet G 1955 *Small-Angle Scattering of X-Rays* (New York: Wiley)
[32] Rintoul R D and Torquato S 1997 *J. Phys. A: Math. Gen.* **30** L585
[33] Bunde A and Havlin S 1996 *Fractals and Disordered Systems* (Berlin: Springer)
[34] Geisler T *et al* unpublished transmission electron microscopic results
[35] Ewing R C, Weber W J and Clinard F W Jr 1995 *Progression Nucl. Energy* **29** 63
[36] Gottfried D, Senftle F E and Waring C L 1956 *Am. Mineral.* **41** 749
[37] Tanabe K and Hiraishi J 1980 *Spectrochim. Acta* **36** 341
[38] Geisler T and Schleicher H 2000 *Chem. Geol.* **163** 269